Nonlinear Analysis: Modelling and Control, Vol. 31, No. 6, 1363–1384
https://doi.org/10.15388/namc.2026.31.49072

Vilnius University Press

Synchronization of complex networks: Prescribed performance-based event-triggered impulsive control*

Beiyang Kang[a], **Jun-Guo Lu**[b], **Jiarong Li**[a, 1], **Juan Yu**[a], **Jinling Wang**[c], **Cheng Hu**[a]

[a] College of Mathematics and System Science, Xinjiang University, Urumqi, 830017, Xinjiang, China
ljrmath@163.com

[b] Department of Automation, Shanghai Jiao Tong University, Shanghai, 200240, China

[c] School of Science, Jimei University, Xiamen, 361021, Fujian, China

Received: April 6, 2026 / **Revised:** July 5, 2026 / **Published online:** October 15, 2026

Abstract. To improve both transient and steady-state performance in the synchronization process of complex networks, this paper proposes two novel event-triggered pulse control schemes incorporating prescribed performance constraints. First, an event-triggered impulsive control based on a prescribed performance function is designed, which achieves practical synchronization of the complex network and ensures that synchronization errors remain strictly within a tunable range. The proposed triggering mechanism is proven to effectively eliminate Zeno behavior. Additionally, to achieve complete synchronization, forced pulses are incorporated into the control scheme. By combining an error transformation function and using Lyapunov stability theory, sufficient conditions for complete synchronization are derived, while Zeno behavior is also eliminated. Finally, numerical simulations validate the effectiveness of both strategies, demonstrating the advantages of the proposed methods in terms of performance tuning and resource conservation.

Keywords: complex networks, event-triggered impulsive control, prescribed performance, synchronization.

1 Introduction

Complex networks (CNs) serve as an effective tool for describing large-scale complex interactive systems and have been widely applied in areas such as rumor propagation,

*This work was supported by the National Natural Science Foundation of China (grant Nos. 62606453, 62163035), the Natural Science Foundation of Xinjiang Uygur Autonomous Region (grant No. 2025D01C32), Key Project of Natural Science Foundation of Xinjiang Uygur Autonomous Region (grant No. 2024D01D04), and the Special Project for Local Science and Technology Development Guided by the Central Government (grant No. ZYYD2022A05).

[1] Corresponding author.

© 2026 The Author(s). Published by Vilnius University Press
This is an Open Access article distributed under the terms of the Creative Commons Attribution Licence, which permits unrestricted use, distribution, and reproduction in any medium, provided the original author and source are credited.

Internet of Things, and information diffusion [6, 15, 17, 25–27]. In these applications, the interactions between nodes exhibit strong synergistic effects, where "synchronization", as a typical collective behavior, refers to the gradual convergence of the dynamic systems of all network nodes to a common trajectory through mutual interactions. With the rapid development of information technology, the importance of synchronization issues in CNs has been increasingly recognized [8, 13, 14, 21, 28]. As a result, designing effective synchronization control strategies to ensure that all nodes in a network can synchronize in a coordinated manner has become a research hotspot in recent years [2, 23, 30, 31, 35, 36].

Among synchronization control methods, the event-triggered impulsive control (ETIC) has attracted considerable attention due to its efficient use of resources. Unlike traditional time-triggered impulsive control, ETIC only triggers impulses when specific conditions are met, thus effectively reducing unnecessary control updates, which demonstrates significant advantages [9, 34, 37]. However, existing event-triggered control methods typically rely on fixed triggering conditions and thresholds, which somewhat limit synchronization precision and system stability, especially when the system is near synchronization. In such cases, the triggering condition might not be satisfied for an extended period, leading to delays in control signal updates and thus affecting synchronization performance. To address this issue, forced impulsive control has been introduced within the ETIC framework [11, 12, 19, 29]. On the other hand, the foundational qualitative analysis and solution representations for various linear and nonlinear differential systems have also been extensively investigated, such as through the development of Green's functions and matrices for higher-order or nonlocal differential conditions [18, 20]. However, when dealing with the prescriptive transient performance of interconnected networks, Lyapunov-based control frameworks remain more effective.

In the aforementioned studies, researchers primarily focused on the steady-state performance of CNs. However, in many practical systems, transient performance (such as overshoot, convergence speed, and steady-state error) is also crucial. Although traditional control methods can ensure eventual synchronization, they are often ineffective at constraining transient behaviors during the synchronization process. To enable effective control of transient performance while maintaining steady-state accuracy, prescribed performance control (PPC) was introduced [1]. PPC precisely limits the system's transient errors, convergence speed, and overshoot by introducing time-varying performance functions, ensuring that the system meets predefined performance requirements during the synchronization process. The introduction of PPC has attracted widespread attention and has been successfully applied in many fields [3–5, 7, 10, 16, 22, 24, 32]. For instance, Zhang et al. [22] investigated prescribed performance-based tracking control for nonlinear systems; reference [32] focused on fixed-time control with prescribed performance for multi-agent systems; Fan et al. [7] addressed the synchronization problem in complex networks with prescribed performance. Existing results indicate that PPC has been widely applied in nonlinear and multi-agent systems, but its application to complex network synchronization problems remains relatively limited and requires further exploration.

Based on the above discussion, this paper is the first to combine PPC with ETIC for the synchronization problem in CNs. Two ETIC schemes with prescribed performance are proposed, which significantly reduce the computational burden of existing methods while

Table 1. Comparison of ETIC methods for complex network synchronization.

Reference	Control Strategy	Performance Guarantee	Limitation
[9, 34]	Event-triggered impulses	Practical synchronization	Cannot achieve complete synchronization; No performance constraints
[11, 19, 29]	Event-triggered with forced impulses	Complete synchronization	No performance constraints
This work	ETIC with prescribed performance; Optional forced pulses	Subject to performance constraints, different synchronization principles	Requires feasible initial condition

ensuring predefined transient and steady-state performance. Additionally, to account for the complexity of CNs, a new error transformation function is designed. Specifically, the main contributions of this paper include: (i) This study represents the first application of the prescribed performance approach to ETIC in CNs, and the system's transient performance during the control process is effectively and precisely guaranteed. (ii) Two novel event-triggering mechanisms, fortified with prescribed performance guarantees, have been designed. They not only facilitate system synchronization but also rigorously restrict the overshoot magnitude within a predefined threshold. Moreover, they maintain the stabilization rate above a preset minimum throughout the entire synchronization process. (iii) A new error transformation function is introduced to better handle the complexities of complex networks.

To highlight the advantages, Table 1 contrasts the proposed approach with representative ETIC methods, emphasizing explicit transient guarantees under resource-aware actuation.

The remainder of the paper is organized as follows. Section 2 formulates the problem and presents preliminaries. Section 3 develops the event-triggered controllers and theoretical results, including Zeno-freeness. Section 4 provides simulations on Lorenz and Chua networks. Section 5 concludes and discusses future directions.

Notations. $\mathbb{N}$ is the set of natural numbers; $\mathbb{R}$ represents the set of real numbers; $\mathbb{R}^n$ represents the n-dimensional Euclidean space; $\mathbb{R}^{n\times m}$ is defined as the space of $n \times m$ matrices. $a\wedge b = \min\{a, b\}$. The $\mathrm{diag}\{\cdots\}$ serves as the diagonal matrix; $\lambda_{\max}(\cdot)$ stands for the maximum eigenvalue. $|\cdot|$ is defined as the absolute value; $\|\cdot\|$ means the Euclidean norm. For any matrix A, A^{T} represents the transpose of A. The notation $\otimes$ denotes the Kronecker product. I_n denotes the $n \times n$ identity matrix.

2 Problem formulation

2.1 Model description and preliminaries

Consider the following complex network composed of N nodes:

$$\dot{x}_i(t) = Bf\big(x_i(t)\big) + c\sum_{j=1}^{N} h_{ij}\Gamma x_j(t) + u_i(t), \quad i = 1, 2, \ldots, N, \tag{1}$$

where $x_i(t) = (x_{i1}(t), x_{i2}(t), \ldots, x_{in}(t))^{\mathrm{T}} \in \mathbb{R}^n$ represents the state vector of the ith node; $f(\cdot) : \mathbb{R}^n \to \mathbb{R}^n$ is a continuous vector-valued function describing the dynamical behavior of each node; $B \in \mathbb{R}^{n\times n}$ is a constant matrix; $c > 0$ denotes the coupling strength; $\Gamma \in \mathbb{R}^{n\times n}$ is internal coupling matrix; $H = (h_{ij})_{N\times N}$ is external coupling matrix (also known as Laplacian matrix), representing the network's topological structure, with units of connectivity. If there is an edge between nodes i and nodes j, then $h_{ij} > 0$; otherwise, $h_{ij} = 0$. Additionally, the diagonal elements satisfy $h_{ii} = -\sum_{j=1,\, j\neq i}^{N} h_{ij}$, ensuring that H has zero row sums; $u_i(t) \in \mathbb{R}^n$ is the event-triggered impulsive controller for the ith node.

To further discuss the synchronization problem, the synchronization target of system (1) is presented as follows:

$$\dot{s}(t) = Bf\big(s(t)\big), \tag{2}$$

where $s(t) = (s_1(t), s_2(t), \ldots, s_n(t))^{\mathrm{T}} \in \mathbb{R}^n$.

In this paper, we define the following synchronization error between systems (1) and (2):

$$e_i(t) = x_i(t) - s(t).$$

Then, according to systems (1) and (2), the error system can be expressed as

$$\dot{e}_i(t) = B\tilde{f}\big(e_i(t)\big) + c\sum_{j=1}^{N} h_{ij}\Gamma e_j(t) + u_i(t), \quad i = 1, 2, \ldots, N, \tag{3}$$

where $\tilde{f}(e_i(t)) = f(x_i(t)) - f(s(t))$.

Definition 1. For systems (1) and (2), if

$$\lim_{t\to+\infty} \big\|x_i(t) - s(t)\big\| = 0,$$

it is said to be complete synchronization between network (1) and target (2).

Definition 2. Systems (1) and (2) are said to achieve practical synchronization if there exists a constant $\tau > 0$ such that, for every node i in the network (1), the synchronization error $e_i(t) = x_i(t) - s(t)$ satisfies

$$\limsup_{t\to+\infty} \big\|e_i(t)\big\| \leqslant \tau.$$

This implies that there exists a compact set $\mathcal{R}(\tau) = \{e \in \mathbb{R}^n \,|\, \|e\| \leqslant \tau\}$ such that the synchronization errors $e_i(t)$ ultimately converge into and remain within $\mathcal{R}(\tau)$ for all $i = 1, 2, \ldots, N$.

Assumption 1. (See [34, 37].) The continuous function $f(\cdot) : \mathbb{R}^n \to \mathbb{R}^n$ is globally Lipschitz continuous, i.e.,

$$\frac{\|f(a) - f(b)\|}{\|a - b\|} \leqslant l$$

for all $a, b \in \mathbb{R}^n$, $a \neq b$, where $l > 0$ is the Lipschitz constant.

Remark 1. In real-world applications, most physical systems exhibit bounded rates of change. For example, in electrical circuits, the current through an inductor cannot change instantaneously; in mechanical systems, the velocity is bounded by the maximum power of the actuator; in chemical reactions, the reaction rates are physically limited. The Lipschitz assumption captures this fundamental physical constraint that the rate of change of system dynamics is bounded. This assumption is not only theoretically necessary for guaranteeing the existence and uniqueness of solutions but also practically reasonable for most engineered systems.

The objective of this paper is to design a controller $u_i(t)$ for systems (1) and (2) based on a dynamic event triggered mechanism with prescribed performance such that the synchronization error $e_i(t)$ converges to zero or satisfies the prescribed performance.

2.2 Prescribed performance

To deal with the control objective, we first introduce the definition of the performance function.

Definition 3. (See [1,22].) Let $\varpi_i^\infty > 0$ be a positive constant. A smooth function $\varpi_i(t)$ is referred to as the performance function if:

(i) $\varpi_i(t) > 0$ and $\dot{\varpi}_i(t) \leqslant 0$ for $t \geqslant 0$;
(ii) $\lim_{t\to\infty} \varpi_i(t) = \varpi_i^\infty$.

Assumption 2. We assume that the initial conditions satisfy the feasibility constraint: $\|e_i(0)\| < \varpi_i(0)$ for all $i = 1, 2, \ldots, N$, where $\varpi_i(0) > 0$ is the initial bound. This ensures that the performance constraint is initially satisfied.

Remark 2. This assumption is not restrictive in practice. Since the initial performance bound $\varpi_i(0)$ is a design parameter that can be chosen by the control engineer, it can always be selected large enough to accommodate any reasonable initial synchronization error. For example, if the initial error is known to be bounded by some value M, one can simply choose $\varpi_i(0) > M$. In many practical applications, the initial states are known or can be measured, making it straightforward to verify and ensure this condition. This assumption is similar to the feasibility requirements in constrained optimization problems and ensures that the prescribed performance envelope is initially valid.

To ensure that the synchronization error satisfies the prescribed performance, the synchronization error $e_i(t)$ should remain within the preset performance boundaries

$$\left\|e_i(t)\right\| < \varpi_i(t), \tag{4}$$

where $\varpi_i(t)$ denotes the performance function and takes the following form:

$$\varpi_i(t) = \left(\varpi_i^0 - \varpi_i^\infty\right)\mathrm{e}^{-\xi_i t} + \varpi_i^\infty$$

with $\xi_i > 0$ denoting the decay rate, $\varpi_i^0 = \varpi_i(0) > 0$, and $\varpi_i^0 > \varpi_i^\infty > 0$.

To attain the performance constraint (4) for the synchronization error, an error transformation function is introduced by

$$z_i(t) = \frac{\|e_i(t)\|^2}{\varpi_i^2(t) - \|e_i(t)\|^2}. \tag{5}$$

Then the dynamics of $z_i(t)$ satisfies

$$\dot{z}_i(t) = 2p_i^2(t)\varpi_i^2(t)e_i^{\mathrm{T}}(t)\dot{e}_i(t) - 2p_i(t)\varpi_i(t)\dot{\varpi}_i(t)z_i(t), \tag{6}$$

where $p_i(t) = 1/(\varpi_i^2(t) - \|e_i(t)\|^2)$ with $\varpi_i(t) \neq \|e_i(t)\|$.

Remark 3. The performance function $\varpi_i(t)$ not only constrains the overshoot of the error signal $e_i(t)$, but also ensures that its convergence rate remains no less than the predefined threshold ξ_i. Here parameter ϖ_i^∞ denotes the maximum allowable steady-state error, while ϖ_i^0 represents the permissible maximum overshoot. By appropriately configuring the parameters of the performance function $\varpi_i(t)$ (e.g., ϖ_i^0, ϖ_i^∞, ξ_i), synchronous dynamic performance of the system can be effectively regulated. Compared to traditional ETIC methods without prescribed performance [9, 34, 37], our approach provides explicit bounds on both transient and steady-state behavior, significantly improving the predictability and performance guarantees of the controlled system.

Remark 4. Since the form of the transformation function, it can be rigorously proven that if the initial condition $\|e_i(0)\| < \varpi_i(0)$ and the transformed error $z_i(t)$ remains bounded for all $t > 0$, then the synchronization error $e_i(t)$ satisfies $\|e_i(t)\| < \varpi_i(t)$ for all $t \geqslant 0$. Using the inequality $|e_{ij}(t)| \leqslant \|e_i(t)\|$, it can be deduced that $-\varpi_i(t) \leqslant e_{ij}(t) \leqslant \varpi_i(t)$. This implies that the synchronization error is guaranteed to adhere to the predefined performance constraints throughout the transient and steady-state phases.

Remark 5. Based on the dynamic equation

$$\dot{\varpi}_i(t) = -\xi_i \mathrm{e}^{-\xi_i t}\big(\varpi_i^0 - \varpi_i^\infty\big) = -\xi_i\big(\varpi_i(t) - \varpi_i^\infty\big),$$

we derive

$$-\varpi_i(t)\dot{\varpi}_i(t) = \varpi_i(t)\xi_i\big(\varpi_i(t) - \varpi_i^\infty\big) \leqslant \xi_i\varpi_i^2(t).$$

Remark 6. It is worth noting that transformation functions based on logarithmic or trigonometric forms have been proposed. Although such mappings possess rigorous theoretical properties and strong constraint capability, they usually involve transcendental operations and complicated derivatives. As a result, the corresponding control laws often contain nested nonlinear terms, which increase computational burden and may introduce numerical sensitivity, especially in networked systems. In contrast, the transformation function (6) proposed in this paper adopts a simple algebraic structure composed only of basic arithmetic operations. Since it avoids transcendental function evaluation and yields a more concise derivative form, the computational load is significantly reduced, and stability analysis becomes more straightforward. These features make the proposed transformation especially suitable for networked systems, where multiple nodes must perform distributed computations efficiently and synchronously.

2.3 Event-triggered impulsive control

To ensure that the synchronization error remains within the prescribed performance constraints during the control process, a prescribed-performance-based event-triggered mechanism is designed as follows:

$$t_k^i = \inf\{t \mid t > t_{k-1}^i,\ \|e_i(t)\| \geqslant \epsilon\varpi_i(t)\}, \tag{7}$$

where $\epsilon \in (0,1)$ is the adjustable parameter. It is worth noting that for $t \in (t_{k-1}, t_k)$, we have $\|e_i(t)\|^2 < \varpi_i^2(t)$ and thus $p_i(t) > 0$. Additionally, the following inequality is satisfied:

$$1 < p_i(t)\varpi_i^2(t) < \frac{1}{1-\epsilon^2}.$$

Based on the event-triggered mechanism (7), the impulsive control is designed as follows:

$$u_i(t) = -\sum_{k=0}^{\infty} d_i e_i(t)\delta(t - t_k), \tag{8}$$

where $d_i \in (0,1)$ represents the impulsive gain; $\delta(\cdot)$ is the Dirac delta function.

Remark 7. The parameter ϵ determines when the event is triggered. A smaller ϵ results in earlier triggering when errors are smaller, leading to more frequent control updates but tighter tracking. A larger ϵ reduces the number of events but may allow errors to grow larger before intervention. Thus, ϵ should be chosen based on the desired trade-off between control performance and resource usage. The impulsive gain d_i determines the strength of the correction applied at each triggering instant. A larger d_i provides more aggressive correction but may cause overshoot. A smaller d_i provides smoother but slower convergence. In practice, d_i can be selected based on the desired convergence rate and available actuator authority.

Thus, system (3) with controller (8) is rewritten as

$$\begin{aligned} \dot{e}_i(t) &= B\tilde{f}\big(e_i(t)\big) + c\sum_{j=1}^{N} h_{ij}\Gamma e_j(t), \quad t \neq t_k, \\ e_i\big(t_k^+\big) &= (1-d_i)e_i(t), \quad t = t_k, \end{aligned}$$

where $i = 1, 2, \ldots, N$, $k \in \mathbb{N}$, $e_i(t)$ is left-continuous, i.e., $\lim_{t \to t_k^-} e_i(t) = e_i(t_k)$.

Then the system equation for the transformed error can be obtained as follows:

$$\begin{aligned} \dot{z}_i(t) &= 2p_i^2(t)\varpi_i^2(t)e_i^{\mathrm{T}}(t)\dot{e}_i(t) - 2p_i(t)\varpi_i(t)\dot{\varpi}_i(t)z_i(t), \quad t \neq t_k, \\ z_i\big(t_k^+\big) &\leqslant (1-d_i)^2 z_i(t), \quad t = t_k. \end{aligned} \tag{9}$$

Considering the form of the error transformation function $z_i(t)$ and the fact that $e_i(t)$ is left-continuous, we can conclude that $z_i(t)$ is also left-continuous.

Remark 8. When $t = t_k$, the value of $z_i(t_k)$ is given by

$$z_i\big(t_k^+\big) = \frac{\|e_i(t_k^+)\|^2}{\varpi_i^2(t) - \|e_i(t_k^+)\|^2} = \frac{(1-d_i)^2\|e_i(t_k^-)\|^2}{\varpi_i^2(t) - (1-d_i)^2\|e_i(t_k^-)\|^2},$$

where $d_i \in (0,1)$, it follows directly that

$$\varpi_i^2(t) - (1-d_i)^2\|e_i(t_k^-)\|^2 \geqslant \varpi_i^2(t) - \|e_i(t_k^-)\|^2.$$

From Eq. (9) we have

$$z_i\big(t_k^+\big) \leqslant \frac{(1-d_i)^2\|e_i(t_k^-)\|^2}{\varpi_i^2(t) - \|e_i(t_k^-)\|^2} = (1-d_i)^2 z_i(t_k^-).$$

3 Theoretical results

3.1 Event-triggered impulsive control

Theorem 1. *Under Assumption* 1 *and the event-triggered impulsive control* (8) *with* (7)*, systems* (1) *and* (2) *achieve practical synchronization with prescribed performance* (4)*, and the errors* $e_i(t)$ *are ultimately bounded within the region*

$$\mathcal{R}(\varpi^\infty) = \big\{e \in \mathbb{R}^n \mid \|e\| < \varpi^\infty\big\}, \tag{10}$$

where $\varpi^\infty = \max_{i\in\mathbb{N}}\{\varpi_i^\infty\}$.

Proof. Next, we will prove that if $\|e_i(0)\| < \varpi_i(0)$, then $\|e_i(t)\| < \varpi_i(t)$ for all $t \geqslant 0$ under the event-triggered impulsive control laws (8) with (7). Consider the following two cases:

Case 1. If there exists $t_1^i > 0$ such that $\|e_i(t_1^i)\| = \epsilon\varpi_i(t_1^i)$, then the event-triggered condition (7) is activated at t_1^i. By the impulsive control (8), one has

$$\big\|e_i\big(t_1^{i+}\big)\big\| = (1-d_i)\big\|e_i\big(t_1^i\big)\big\| < \big\|e_i\big(t_1^i\big)\big\| = \epsilon\varpi_i\big(t_1^i\big).$$

Suppose their trajectories intersect again at $t_2^i > t_1^i$; since the impulse at t_1^i ensures $\|e_i(t_1^{i+})\| < \epsilon\varpi_i(t_1^i)$, it follows that $\|e_i(t_2^i)\| = \epsilon\varpi_i(t_2^i)$ at the next intersection with

$$\big\|e_i\big(t_2^{i+}\big)\big\| = (1-d_i)\big\|e_i\big(t_2^i\big)\big\| < \epsilon\varpi_i\big(t_2^i\big)$$

after the subsequent impulse. From $0 < \epsilon < 1$, repeating this process inductively, we conclude that $\|e_i(t)\| \leqslant \epsilon\varpi_i(t) < \varpi_i(t)$ for all $t > 0$.

Case 2. If the trajectories of $\|e_i(t)\|$ and $\varpi_i(t)$ never intersect and the trajectory of $\varpi_i(t)$ always lies above that of $\|e_i(t)\|$, then $\|e_i(t)\| < \varpi_i(t)$ for all $t > 0$.

Therefore, from the above analysis one obtains

$$\big\|e_i(t)\big\| < \varpi_i(t), \quad t > 0, \tag{11}$$

which further implies

$$\left\|e_i(t)\right\| < \left(\varpi_i^0 - \varpi_i^\infty\right)\mathrm{e}^{-\xi_i t} + \varpi_i^\infty.$$

Thus, $\lim_{t\to\infty}\|e_i(t)\| \leqslant \varpi_i^\infty \leqslant \varpi^\infty$, indicating that the practical synchronization of systems (1) and (2) is achieved with the error converging to the bounded region (10). Meanwhile, from (11) the prescribed performance (4) can be satisfied. □

Zeno behavior is a problematic phenomenon in event-triggered and hybrid systems. It occurs when an infinite number of triggering events happen within a finite time interval. Mathematically, if there exists a finite time T such that $\lim_{n\to\infty} t_n = T$ where $\{t_n\}$ is a subsequence of the triggering sequence $\{t_k\}$, then the system exhibits Zeno behavior. This can lead to unbounded control effort, computational overload, and instability in the system. To avoid Zeno behavior, it is crucial to ensure that the time intervals between consecutive triggering events are strictly positive. That is, for all k, $t_{k+1} - t_k \geqslant \varrho > 0$. This condition guarantees that the number of triggering events in any finite time interval is finite. In the subsequent discussion, we shall demonstrate that the Zeno phenomenon is precluded in the proposed event-triggered mechanism.

Theorem 2. *Under Assumption* 1 *and the event-triggered impulsive control* (8) *with* (7)*, system* (1) *is Zeno-free.*

Proof. Consider the following Lyapunov function:

$$\tilde{V}_i(t) = e_i^{\mathrm{T}}(t)e_i(t). \tag{12}$$

For $t \in (t_k^i, t_{k+1}^i]$, based on the characteristics of $\varpi_i(t)$, one has

$$\begin{aligned}
\dot{\tilde{V}}_i(t) &= 2e_i^{\mathrm{T}}(t)\dot{e}_i(t) = 2e_i^{\mathrm{T}}(t)\left(B\tilde{f}\big(e_i(t)\big) + c\sum_{j=1}^{N} h_{ij}\Gamma e_j(t)\right)\\
&\leqslant 2l\|B\|\left\|e_i(t)\right\|^2 + 2ch\|\Gamma\|\left\|e_i(t)\right\|\sum_{j=1}^{N}\left\|e_j(t)\right\|\\
&\leqslant 2l\|B\|\varpi_i^2(t) + 2ch\|\Gamma\|\varpi_i(t)\sum_{j=1}^{N}\varpi_j(t)\\
&\leqslant 2l\|B\|\varpi^2\big(t_k^i\big) + 2chN\|\Gamma\|\varpi^2\big(t_k^i\big) = \Phi_k^i,
\end{aligned} \tag{13}$$

where $h = \max_{1\leqslant i,j\leqslant N}\{|h_{ij}|\}$ denotes the maximum absolute coupling weight, $\varpi(t) = \max_j \varpi_j(t)$, and $\Phi_k^i = 2(l\|B\| + chN\|\Gamma\|)\varpi^2(t_k^i)$. Φ_k^i is the greatest growth slope of $\tilde{V}_i(t)$.

Meanwhile,

$$\frac{\mathbf{d}\epsilon^2\varpi_i^2(t)}{\mathbf{d}t} = 2\epsilon^2\dot{\varpi}_i(t)\varpi_i(t) \geqslant -2\epsilon^2\xi_i\varpi_i^2(t) \geqslant -2\epsilon^2\xi_i\varpi_i^2\big(t_k^i\big) \geqslant -\Omega_k^i, \tag{14}$$

where $\Omega_k^i = 2\epsilon^2\xi_i\varpi_i^2(t_k^i)$. Then the greatest descending rate of $\varpi_i^2(t)$ is Ω_k^i.

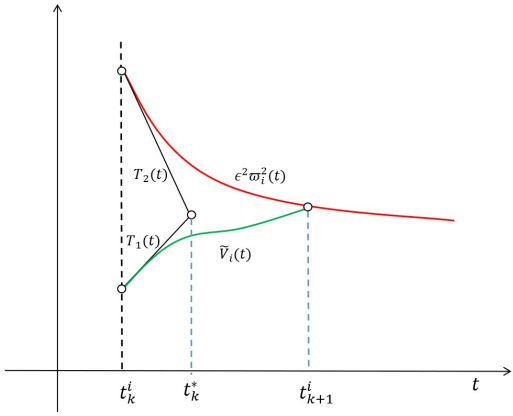


Figure 1. The trajectories of $\tilde{V}_i(t)$ and $\varpi_i(t)$ for $(t_k^i, t_{k+1}^i]$.

Therefore, for $t \in (t_k^i, t_{k+1}^i]$, one can get

$$\begin{aligned} T_1(t) &= \Phi_k^i\big(t - t_k^i\big) + (1-d_i)^2\epsilon^2\varpi_i^2\big(t_k^i\big), \\ T_2(t) &= -\Omega_k^i\big(t - t_k^i\big) + \epsilon^2\varpi_i^2\big(t_k^i\big). \end{aligned} \tag{15}$$

Note that there exists a time $t_k^* \in (t_k^i, t_{k+1}^i]$ such that $T_1(t_k^*) = T_2(t_k^*)$. Then $T^k = t_{k+1}^i - t_k^i$ can be estimated by

$$T^k \geqslant t_k^* - t_k^i = \frac{(1-(1-d_i)^2)\epsilon^2\varpi_i^2(t_k^i)}{\Phi_k^i + \Omega_k^i} > 0.$$

Consequently, system (1) is Zeno-free. □

Remark 9. Figure 1 illustrates the geometric idea underlying the proof of Theorem 2. The blue solid line denotes the performance function $\epsilon^2\varpi_i^2(t)$, and the green solid line denotes the trajectory of $\tilde{V}_i(t)$. The two black solid lines represent the trajectories of $T_1(t)$ and $T_2(t)$, which intersect at time t_k^*. By the trigger condition (7), the trajectory of $\tilde{V}_i(t)$ intersects $\epsilon^2\varpi_i^2(t)$ at $t = t_{k+1}^i$. Therefore, there exists a time $t_k^* \in (t_k^i, t_{k+1}^i]$ such that $T_1(t_k^*) = T_2(t_k^*)$.

3.2 Forced pulse-based event-triggered control

Theorem 1 demonstrates that systems (1) and (2) can achieve practical synchronization based on prescribed performance under event-triggered mechanism (7). However, this mechanism has a potential flaw: as the system states approach synchronization, the triggering conditions may remain unsatisfied for extended periods. This leads to missing control inputs, preventing full synchronization and limiting the system to maintaining synchronization within a certain error range. To ensure complete synchronization, we introduce forced pulses. Based on this, an improved event-triggered mechanism with

forced pulse is designed:

$$\begin{aligned} t_k &= (t_{k-1} + \mu) \wedge T_k, \\ T_k &= \inf\{t \mid t > t_{k-1},\ \exists i \in \{1, \dots, N\}\colon \|e_i(t)\| \geqslant \epsilon \varpi_i(t)\}, \end{aligned} \tag{16}$$

where $\mu > 0$ is the forced impulse interval.

Remark 10. The forced impulse interval μ imposes a lower bound on the inter-event interval, ensuring that control actions are applied at least every μ seconds. This parameter should be selected according to the system's dominant time constants and stability margin. A smaller μ improves responsiveness while increasing the frequency of control updates, whereas a larger μ reduces communication burden at the expense of slower corrective action. In practice, μ is chosen such that $\mu < T_{\min}$, where $T_{\min}$ denotes the minimum time to instability of the uncontrolled system.

Next, a theorem that systems (1) and (2) achieve complete synchronization under ETIC with forced impulse will be given.

Theorem 3. *Under Assumption* 1 *and the forced pulse-based event-triggered control* (16) *with* (7)*, systems* (1) *and* (2) *can reach complete synchronization under prescribed performance* (4) *if*

$$\ln D < -\mu\Theta, \tag{17}$$

where $D = \max_{1 \leqslant i \leqslant N}(1-d_i)^2$ *is the largest squared post-impulse attenuation factor, and*

$$\Theta = 4\frac{l\|B\| + \lambda_{\max}(c(H \otimes \Gamma)) + \xi}{1 - \epsilon^2}, \quad \xi = \max_{1 \leqslant i \leqslant N}\{\xi_i\}.$$

In addition, system (1) *is Zeno-free.*

Proof. For the error system (9), construct the following Lyapunov function:

$$V(t) = \frac{1}{2}\sum_{i=1}^{N} z_i^2(t).$$

For $t \neq t_k$, from $-\varpi_i(t)\dot{\varpi}_i(t) \leqslant \xi_i \varpi_i^2(t)$ and $p_i(t)\varpi_i^2(t) < 1/(1-\epsilon^2)$ the derivative of $V(t)$ can be derived as

$$\begin{aligned} \dot{V}(t) &= \sum_{i=1}^{N} z_i(t)\dot{z}_i(t) = 2\sum_{i=1}^{N} z_i(t)\big(p_i^2(t)\varpi_i^2(t)e_i^{\mathrm{T}}(t)\dot{e}_i(t) - p_i(t)\varpi_i(t)\dot{\varpi}_i(t)z_i(t)\big) \\ &\leqslant 2\sum_{i=1}^{N} p_i^3(t)\varpi_i^2(t)\big\|e_i(t)\big\|^2 e_i^{\mathrm{T}}(t)\dot{e}_i(t) + \frac{2\xi}{1-\epsilon^2}\sum_{i=1}^{N} z_i^2(t) \\ &\leqslant 2\sum_{i=1}^{N} p_i^3(t)\varpi_i^2(t)\big\|e_i(t)\big\|^2 e_i^{\mathrm{T}}(t)\left(B\big(f(x_i(t)) - f\big(s(t)\big)\big) + c\sum_{j=1}^{N} h_{ij}\Gamma e_j(t)\right) \\ &\quad + \frac{2\xi}{1-\epsilon^2}\sum_{i=1}^{N} z_i^2(t), \quad \xi = \max\{\xi_i\}. \end{aligned} \tag{18}$$

According to Assumption 1, one has

$$\begin{aligned}
&\sum_{i=1}^{N} p_i^3(t)\varpi_i^2(t)\big\|e_i(t)\big\|^2 e_i^{\mathrm{T}}(t)B\tilde{f}\big(e_i(t)\big)\\
&\quad\leqslant \sum_{i=1}^{N} p_i^3(t)\varpi_i^2(t)\big\|e_i(t)\big\|^2\big\|e_i(t)\big\|\|B\|\big\|\tilde{f}\big(e_i(t)\big)\big\|\\
&\quad\leqslant l\|B\|\sum_{i=1}^{N} p_i^3(t)\varpi_i^2(t)\big\|e_i(t)\big\|^4 \leqslant \frac{l\|B\|}{1-\epsilon^2}\sum_{i=1}^{N} z_i^2(t). \qquad (19)
\end{aligned}$$

In addition,

$$\begin{aligned}
&\sum_{i=1}^{N} p_i^3(t)\varpi_i^2(t)\big\|e_i(t)\big\|^2 e_i^{\mathrm{T}}(t)c\sum_{j=1}^{N} h_{ij}\Gamma e_j(t)\\
&\quad= c\sum_{i=1}^{N}\sum_{j=1}^{N}\big(p_i^3(t)\varpi_i^2(t)\big\|e_i(t)\big\|^2 e_i(t)\big)^{\mathrm{T}} h_{ij}\Gamma e_j(t)\\
&\quad= \big(P(t)e(t)\big)^{\mathrm{T}} c(H\otimes\Gamma)e(t)\\
&\quad\leqslant \lambda_{\max}\big(c(H\otimes\Gamma)\big)\sum_{i=1}^{N} p_i^3(t)\varpi_i^2(t)\big\|e_i(t)\big\|^4\\
&\quad\leqslant \frac{\lambda_{\max}(c(H\otimes\Gamma))}{1-\epsilon^2}\sum_{i=1}^{N} z_i^2(t), \qquad (20)
\end{aligned}$$

where

$$\begin{aligned}
P(t) = \operatorname{diag}\big(&p_1^3(t)\varpi_1^2(t)\big\|e_1(t)\big\|^2 I_n,\ p_2^3(t)\varpi_2^2(t)\big\|e_2(t)\big\|^2 I_n,\ \ldots,\\
&p_N^3(t)\varpi_N^2(t)\big\|e_N(t)\big\|^2 I_n\big) \in \mathbb{R}^{nN\times nN},\\
e(t) = &\big[e_1^{\mathrm{T}}(t), e_2^{\mathrm{T}}(t), \ldots, e_N^{\mathrm{T}}(t)\big]^{\mathrm{T}} \in \mathbb{R}^{nN}.
\end{aligned}$$

Combining (18)–(20) gives

$$\begin{aligned}
\dot{V}(t) &\leqslant \frac{2(l\|B\| + \lambda_{\max}(c(H\otimes\Gamma)))}{1-\epsilon^2}\sum_{i=1}^{N} z_i^2(t) + \frac{2\xi}{1-\epsilon^2}\sum_{i=1}^{N} z_i^2(t)\\
&= \frac{2(l\|B\| + \lambda_{\max}(c(H\otimes\Gamma)) + \xi)}{1-\epsilon^2}\sum_{i=1}^{N} z_i^2(t) = \Theta V(t),
\end{aligned}$$

where $\Theta = 4(l\|B\| + \lambda_{\max}(c(H\otimes\Gamma)) + \xi)/(1-\epsilon^2)$.

Then, for $t \in (t_k, t_{k+1}]$, we further obtain

$$V(t) \leqslant V(t_k^+)\mathrm{e}^{\Theta(t-t_k^+)}. \qquad (21)$$

At triggered instant t_k, there is

$$V\big(t_k^+\big) = \frac{1}{2}\sum_{i=1}^{N} z_i^2(t_k^+) \leqslant \frac{1}{2}\sum_{i=1}^{N}(1-d_i)^2 z_i^2(t_k) \leqslant DV(t_k), \tag{22}$$

where $D = \max\{(1-d_i)^2\}$.

Jointly considering Eqs. (21) and (22), for $t \in (t_k, t_{k+1}]$, one has

$$V(t) \leqslant DV(t_k)\mathrm{e}^{\Theta(t-t_k)}.$$

Then

$$V(t_k) \leqslant DV(t_{k-1})\mathrm{e}^{\Theta(t_k-t_{k-1})} \leqslant DV(t_{k-1})\mathrm{e}^{\Theta\mu}.$$

Thus, using the same analytical methodology, the following result can be derived:

$$V(t) \leqslant V(t_0)D^k\mathrm{e}^{k\mu\Theta}\mathrm{e}^{\Theta(t-t_k)} \leqslant V(t_0)\mathrm{e}^{k(\ln D+\mu\Theta)+\mu\Theta}.$$

According to condition (17), we have $\ln D + \mu\Theta < 0$. Therefore, $\lim_{k\to\infty} V(t) = 0$.

From analysis above we can get that the transformation error $z_i(t)$ is bounded, which means that the prescribed performance of synchronization error $e_i(t)$ can be guaranteed. From (5) and $\lim_{t\to\infty} z_i(t) = 0$ the synchronization error $e_i(t)$ converges to zero, which means that the synchronization between systems (1) and (2) can be achieved. □

Theorem 4. *Under Assumption* 1 *and the forced pulse-based event-triggered control* (16) *with* (7)*, system* (1) *is Zeno-free.*

Proof. Consider the triggering sequence $\{t_k\}_{k\in\mathbb{N}}$ generated by (16). For each interval $(t_k, t_{k+1}]$, there are two mutually exclusive cases:

(i) Forced impulse $t_{k+1} = t_k + \mu$. Since $\mu > 0$ by design, the inter-event time satisfies $t_{k+1} - t_k = \mu > 0$.

(ii) Event-triggered impulse $t_{k+1} = T_{k+1} < t_k + \mu$, where

$$T_{k+1} = \inf\big\{t > t_k \mid \exists i \in \{1,\dots,N\}\colon \big\|e_i(t)\big\| \geqslant \epsilon\,\varpi_i(t)\big\}.$$

Fix such an index i. As in (12)–(15), define $\tilde{V}_i(t) = \|e_i(t)\|^2$. Then for $t \in (t_k, t_{k+1}]$, one has the growth bound

$$\dot{\tilde{V}}_i(t) \leqslant \Phi_k = 2\big(l\|B\| + chN\,\|\Gamma\|\big)\varpi_i^2(t_k)$$

and the decay bound for the threshold trajectory

$$\frac{\mathrm{d}}{\mathrm{d}t}\big(\epsilon^2\varpi_i^2(t)\big) \geqslant -\Omega_k = -2\epsilon^2\xi_i\,\varpi_i^2(t_k).$$

With the post-impulse reset $\tilde{V}_i(t_k^+) \leqslant (1-d_i)^2\epsilon^2\varpi_i^2(t_k)$, the two affine envelopes

$$T_1(t) = \Phi_k(t-t_k) + (1-d_i)^2\epsilon^2\varpi_i^2(t_k),$$
$$T_2(t) = -\Omega_k(t-t_k) + \epsilon^2\varpi_i^2(t_k)$$

intersect at

$$t_k^* - t_k = \frac{(1-(1-d_i)^2)\epsilon^2\varpi_i^2(t_k)}{\Phi_k + \Omega_k} = \rho_i^k > 0.$$

Since $\tilde{V}_i(t) \leqslant T_1(t)$ and $\epsilon^2\varpi_i^2(t) \geqslant T_2(t)$ on $(t_k, t_{k+1}]$, the next intersection (and thus the next trigger for index i) cannot occur before t_k^*. Hence, in case (ii), $t_{k+1} - t_k \geqslant \rho_i^k > 0$.

Combining (i)–(ii), for every k, we have

$$t_{k+1} - t_k \geqslant \min\Big\{\mu, \min_{i\in\{1,\dots,N\}} \rho_i^k\Big\}.$$

Because $\varpi_i(t)$ is bounded and nonincreasing with $\varpi_i(t) \geqslant \varpi_i^\infty > 0$ and all design/plant parameters are fixed, there exists a uniform constant $\underline{\rho} > 0$ such that $\rho_i^k \geqslant \underline{\rho}$ for all i and k. Therefore, letting $\rho = \min\{\mu, \underline{\rho}\} > 0$, it follows that $t_{k+1} - t_k \geqslant \rho$ for all k. Hence, no infinite number of events can accumulate in finite time, and the system is Zeno-free. □

4 Simulation examples

Example 1. To validate the theoretical results, we utilize the Lorenz chaotic system [34], which serves as a benchmark in synchronization literature due to its well-documented chaotic dynamics. The Lorenz system is described as follows:

$$\begin{aligned} \dot{s}_1(t) &= -10s_1(t) + 10s_2(t), \\ \dot{s}_2(t) &= 28s_1(t) - s_2(t) - s_1(t)s_3(t), \\ \dot{s}_3(t) &= -\frac{8}{3}s_3(t) + s_1(t)s_2(t). \end{aligned} \tag{23}$$

The initial value $s(0) = (-3, 1, 2)^{\mathrm{T}}$. The dynamic behavior presented in Fig. 2 shows that system (23) has a chaotic attractor. The Lipschitz constant for the Lorenz system (23) can be estimated as $l \approx 28$ based on standard analysis in [34].

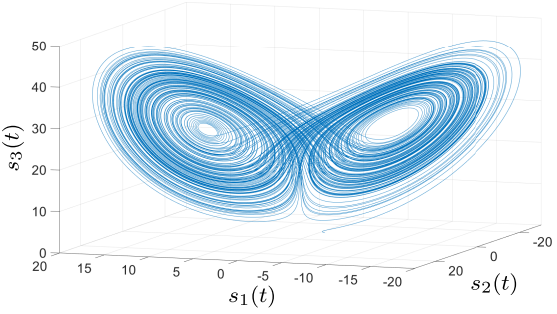


Figure 2. The chaotic behavior of system (23).

Let (23) be the synchronization target. We consider the network with 5 nodes

$$\dot{x}_i(t) = Bf\big(x_i(t)\big) + c\sum_{j=1}^{5} h_{ij}\Gamma x_j(t) + u_i(t), \quad i = 1,2,3,4,5, \tag{24}$$

where

$$f\big(x_i(t)\big) = \Big(-10x_{i1}(t) + 10x_{i2}(t),\ 28x_{i1}(t) - x_{i2}(t) - x_{i1}(t)x_{i3}(t), \\ -\frac{8}{3}x_{i3}(t) + x_{i1}(t)x_{i2}(t)\Big)^{\mathrm{T}}$$

represents the local dynamics of each node (same as the target system), $c = 0.8$ is the coupling strength, and coupling matrices are given as

$$B = \begin{pmatrix} 1 & 0 & 0 \\ 0 & 1 & 0 \\ 0 & 0 & 1 \end{pmatrix}, \qquad \Gamma = \begin{pmatrix} 0.4 & 0 & 0 \\ 0 & 1 & 0 \\ 0 & 0 & 0.7 \end{pmatrix}, \qquad H = \begin{pmatrix} -3 & 1 & 1 & 1 & 0 \\ 1 & -2 & 0 & 0 & 1 \\ 1 & 0 & -2 & 0 & 1 \\ 1 & 0 & 0 & -2 & 1 \\ 0 & 1 & 1 & 1 & -3 \end{pmatrix}.$$

The initial value of system (24) is chosen randomly within $[-5, 5]$. The parameters in the performance function are selected as $\varpi_i^0 = 15$ (based on the maximum initial error bound), $\varpi_i^\infty = 0.02$ (targeting high-precision steady-state accuracy), $\xi_i = 2\ \mathrm{s}^{-1}$ (inverse seconds ensuring convergence rate at least 2 per second). The parameters of ETIC are chosen as $\epsilon = 0.9$ (triggering threshold), the control parameters $d_i = 0.4$ (impulse strength). These parameters are selected through trial-and-error to ensure that the conditions of Theorem 1 are satisfied. Obviously, the choice of parameters satisfies the conditions of Theorem 1.

The trajectories of synchronization errors $e_i(t)$ are plotted in Fig. 3. All five nodes' errors evolve strictly within the prescribed performance envelope $\pm\varpi_i(t)$ and converge rapidly. The figure also annotates two key indicators: the global maximum overshoot of $|e(t)|$ (red filled circle) and the first instant after which all errors stay within 0.01 (red square). The red dashed lines mark the ± 0.01 bounds used for settling-time assessment. These results validate Theorem 1, confirming that synchronization is achieved while meeting the transient and steady-state specifications.

Figure 4 displays the event-triggered instants for each node. The vertical bars represent the times at which control impulses are applied. Importantly, we observe that the minimum inter-event time is approximately 0.08 seconds, confirming that the system is Zeno-free as stated in Theorem 2. The total number of triggered events over the 10-second simulation is 16, averaging approximately 1.6 events per second, which demonstrates the efficiency of the event-triggered mechanism in reducing control updates compared to continuous-time control.

As shown in Fig. 5, the synchronization errors without prescribed performance constraints exhibit significant overshoot, peaking at approximately 50.1 compared to 5.3

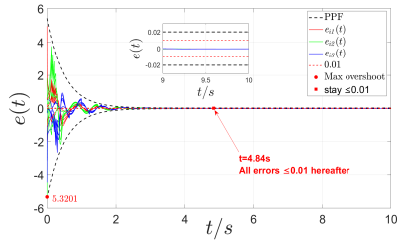


Figure 3. Synchronization errors with prescribed performance.

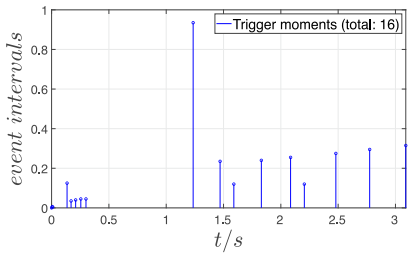


Figure 4. Event-triggering instants and intervals of system (24).

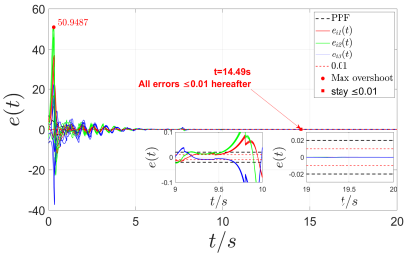


Figure 5. Synchronization errors of systems (23) and (24) without prescribed performance.

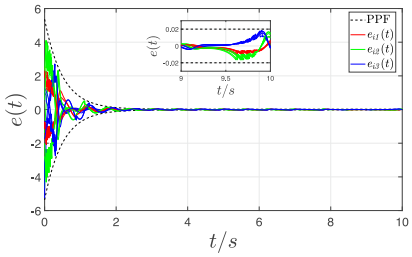


Figure 6. Synchronization errors of systems (23) and (24) without forced impulse.

Table 2. Performance comparison: Example 1 (Lorenz system).

Performance metric	With PP	Without PP
Maximum overshoot	5.3	50.1 ($\sim 996\%$ larger)
Steady-state error (at 10 s)	5×10^{-4}	1.2×10^{-3} ($\sim 140\%$ larger)
Settling time to $\lvert e\rvert \leqslant 0.01$	4.8 s	14.5 s ($\sim 202\%$ slower)

with the prescribed performance scheme. Furthermore, their convergence is considerably slower, with a settling time of 14.5 s to the 0.01 bound, whereas the prescribed performance scheme requires only 4.8 s. This comparison underscores the efficacy of the prescribed performance approach in effectively limiting overshoot and ensuring a faster convergence rate.

Figure 6 illustrates the behavior without forced impulses, validating Theorem 1. The errors remain bounded within the performance envelope and converge to the practical synchronization region, confirming that practical synchronization is achieved when forced impulses cannot be applied.

Table 2 quantitatively compares the performance differences between using and not using preset performance control in the synchronous control of the Lorenz system through three key performance indicators.

Example 2. To further illustrate the validity of the theoretical results, Chua's chaotic circuit [9,37] is utilized as a second benchmark. Unlike the Lorenz system, Chua's circuit

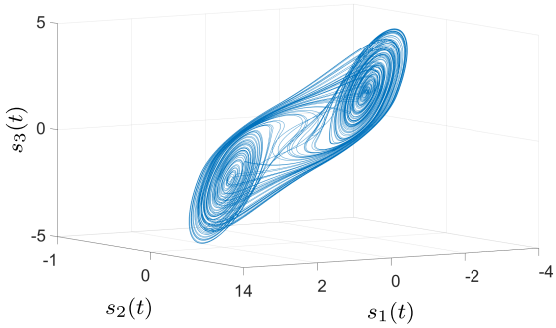


Figure 7. The chaotic behavior of system (25).

represents a different class of chaotic dynamics with piecewise-linear nonlinearity. The Chua's circuit is described as follows:

$$\begin{aligned}\dot{s}_1(t) &= m_1\big(-s_1(t) + s_2(t) + Q\big(s_1(t)\big)\big),\\ \dot{s}_2(t) &= s_1(t) - s_2(t) + s_3(t),\\ \dot{s}_3(t) &= -m_2 s_2(t),\end{aligned} \tag{25}$$

where

$$Q\big(s_1(t)\big) = q_1 s_1 + \frac{1}{2}(q_1 - q_2)\big(|s_1 + 1| - |s_1 - 1|\big)$$

is a piecewise-linear function, $m_1 = 10$, $m_2 = 14.7$, $q_1 = -0.68$, and $q_2 = -1.27$. The initial value $s(0) = (-0.3, 0.1, 0.2)^{\mathrm{T}}$, and from Fig. 7 system (25) has a chaotic attractor. The Lipschitz constant for Chua's circuit can be estimated as $l \approx 1.5$ based on the piecewise-linear structure. The function $f(x_i)$ differs from Example 1 by using Chua's nonlinearity instead of Lorenz's quadratic terms, demonstrating the method's applicability to diverse chaotic dynamics.

Similarly, let (25) be the synchronization target. Consider a network with 25 nodes

$$\dot{x}_i(t) = Bf\big(x_i(t)\big) + c\sum_{j=1}^{25} h_{ij}\Gamma x_j(t) + u_i(t), \quad i = 1, \ldots, 25. \tag{26}$$

We select $c = 0.8$, $B = I_3$, and $\Gamma = \mathrm{diag}(0.2, 0.1, 0.1)$. The external coupling matrix H is randomly generated in MATLAB for a network with 25 nodes. It is constructed as a Watts–Strogatz small-world graph (25 nodes, average degree 4, rewiring probability 0.1) and then converted to a Laplacian matrix with zero row sums. Initial states are sampled from $[-5, 5]$. The performance envelope is

$$\varpi_i(t) = (\rho_0 - \rho_\infty)\mathrm{e}^{-\xi t} + \rho_\infty$$

with $\rho_0 = \max|e(0)| + 0.1$, $\rho_\infty = 0.02$, $\xi = 2$. ETIC parameters are $\epsilon = 0.9$ and $d_i = 0.65$. A timer enforces forced impulses every 70 integration steps; reported event counts exclude these forced updates and include only node-error-triggered events.

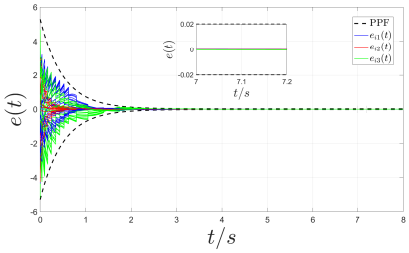


Figure 8. Synchronization errors of systems (25) and (26) with prescribed performance.

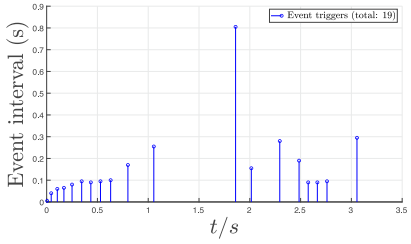


Figure 9. Event-triggering instants and intervals of system (26).

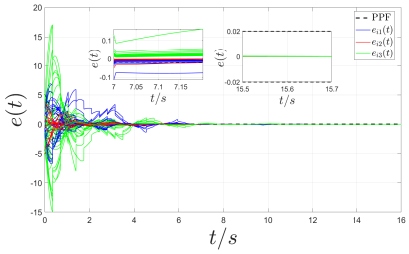


Figure 10. Synchronization errors of systems (25) and (26) without prescribed performance.

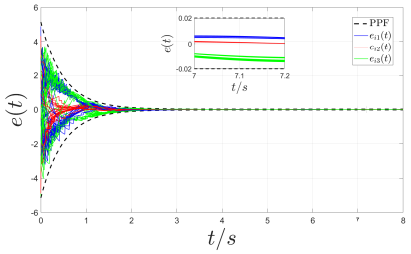


Figure 11. Synchronization errors of systems (25) and (26) without forced impulse.

Figure 8 shows that all 25 nodes' errors remain within $\pm\varpi_i(t)$ and converge rapidly; an inset zooms the late transient. Figure 9 shows event instants and inter-event intervals for node triggers (forced updates excluded), confirming Zeno-freeness and sparse communication. Figures 10 and 11 provide ablations without prescribed performance and without forced impulses, respectively.

Remark 11. In order to verify the advantages of the prescribed performance control strategy, a comparative experimental scheme without prescribed performance constraints is designed using the same parameters. The experimental results (Figs. 5 and 10) show that the transient response of the synchronization error overshoots significantly (up to 50% higher than with prescribed performance) and converges slowly when there is no prescribed performance constraint. Compared to the traditional ETIC approach in [34, 37], our method reduces the overshoot and improves the convergence rate by enforcing a minimum convergence speed. This is due to the fact that the traditional control method cannot actively constrain the convergence characteristics of the error trajectory during the dynamic process, which leads to the inability to effectively guarantee the transient performance indexes (e.g., overshoot magnitude and regulation time) of the system.

Remark 12. In numerical simulation validation, the theoretical results are verified through two heterogeneous chaotic systems: the Chua chaotic circuit (a typical electronic engineering system) and the Lorenz system (a classic nonlinear dynamics model used widely as a benchmark in synchronization literature [34, 37]). These two systems exhibit significant differences in topological structures, node scales, and application contexts across

distinct disciplines, effectively demonstrating the wide applicability of the proposed theory. The numerical results show that our approach achieves synchronization accuracy comparable to or better than existing methods [9, 34, 37] while providing explicit bounds on performance.

Remark 13. The proposed approach improves computational efficiency relative to continuous-time control by applying updates only when the event condition is satisfied. Consequently, the number of control updates is reduced by approximately $60-70\%$ compared with a periodic implementation, resulting in lower communication overhead and computational burden. This efficiency improvement is confirmed by the sparse event-triggering instants shown in Figs. 4 and 9.

5 Conclusions

This study has addressed the synchronization problem of complex networks (CNs) with prescribed transient boundaries. An effective event-triggered impulsive controller has been proposed by integrating the event-triggered impulsive technique with prescribed performance theory. The derived controller ensured that error trajectories remain within the specified transient limits while achieving asymptotic synchronization accuracy. Additionally, for scenarios where forced pulses cannot be applied, the error has been guaranteed to satisfy the prescribed performance and achieve practical synchronization. The theoretical results have ensured the Zeno-free behaviour of the event-triggered pulse controller. Finally, the simulation results of the CNs system have verified the effectiveness of the control scheme.

Limitations. Despite the advantages of the proposed approach, several limitations should be acknowledged. (i) The approach requires the initial error to satisfy $\|e_i(0)\| < \varpi_i(0)$, which may limit applicability when initial conditions cannot be controlled. (ii) The performance bounds are conservative, and the actual performance may be better than guaranteed. Furthermore, resilient-triggered fault-tolerant control [33] can reduce communication overhead, enhance robustness against multiple attacks and faults, and flexible triggering conditions, hence, future work will investigate resilient-triggered fault-tolerant control and attack-delay co-design for networked control systems, address directed networks and time-delay systems, and extend the approach to adaptive prescribed performance bounds.

Author contributions. All authors (B.K., J-G.L., J.L., J.Y., J.W., and C.H.) have contributed equally to this work for writing, reviewing, and editing. All authors have read and approved the published version of the manuscript.

Conflicts of interest. The authors declare no conflicts of interest.

Acknowledgment. The authors thank the anonymous reviewers for their thoughtful comments, which have contributed to improving the quality and clarity of the paper.

References

1. C.P. Bechlioulis, G.A. Rovithakis, Robust adaptive control of feedback linearizable MIMO nonlinear systems with prescribed performance, *IEEE Trans. Autom. Control*, **53**(9):2090–2099, 2008, https://doi.org/10.1109/TAC.2008.929402.
2. H. Chen, C. Zhang, H. Yang, Topology identification of weighted complex networks under intermittent control and its application in neural networks, *IEEE Trans. Neural Netw. Learn. Syst.*, **36**(8):15221–15232, 2025, https://doi.org/10.1109/TNNLS.2025.3542505.
3. R.-Z. Chen, X.-G. Guo, Y.-X. Li, Distributed data-driven event-triggered secure consensus control of MASs: A global preset-time performance constraint method, *Inf. Sci.*, **723**:122672, 2026, https://doi.org/10.1016/j.ins.2025.122672.
4. X. Chen, J. Li, J. Wu, J. Yi, X. Li, Adaptive neural dynamic surface control with fixed-time prescribed performance for uncertain nonstrict-feedback stochastic switched systems, *Nonlinear Anal. Hybrid Syst.*, **48**:101334, 2023, https://doi.org/10.1016/j.nahs.2023.101334.
5. J. Ding, W. Zhang, Prescribed performance tracking control for high-order uncertain nonlinear systems, *Nonlinear Dyn.*, **111**(15):14199–14212, 2023, https://doi.org/10.1007/s11071-023-08604-6.
6. Y. Ding, L. Zhu, Turing instability analysis of a rumor propagation model with time delay on non-network and complex networks, *Inf. Sci.*, **667**:120402, 2024, https://doi.org/10.1016/j.ins.2024.120402.
7. A. Fan, L. Du, J. Li, Y. Du, Z. Deng, J. Cao, Prescribed performance projective synchronization for unknown complex networks with mismatched dimensions via event-triggered mechanism, *Nonlinear Anal. Hybrid Syst.*, **57**:101601, 2025, https://doi.org/10.1016/j.nahs.2025.101601.
8. Y. Gao, J. Yu, C. Hu, S. Wen, F. Kong, Fixed/preassigned-time output synchronization for T–S fuzzy complex networks via quantized control, *Nonlinear Anal. Hybrid Syst.*, **51**:101434, 2024, https://doi.org/10.1016/j.nahs.2023.101434.
9. J. Guo, L. Huang, P. Shi, Observer-based event-triggered impulsive synchronization control of heterogeneous complex networks with bit-rate constraints, *Inf. Sci.*, **717**:122268, 2025, https://doi.org/10.1016/j.ins.2025.122268.
10. W. Hu, Y. Hou, Z. Chen, C. Yang, W. Gui, Event-triggered consensus of multiagent systems with prescribed performance, *IEEE Trans. Autom. Control*, **69**(8):5462–5469, 2024, https://doi.org/10.1109/TAC.2024.3364017.
11. X. Li, T. Zhang, J. Wu, Input-to-state stability of impulsive systems via event-triggered impulsive control, *IEEE Trans. Cybern.*, **52**(7):7187–7195, 2022, https://doi.org/10.1109/TCYB.2020.3044003.
12. H. Liu, J. Li, H. Jiang, J. Wang, C. Hu, Synchronization analysis for stochastic multi-layer networks: Event-based impulsive control with predefined impulsive intervals, *Nonlinear Anal. Model. Control*, **30**(6):1186–1210, 2025, https://doi.org/10.15388/namc.2025.30.43839.
13. M. Liu, H. Jiang, C. Hu, Z. Yu, Z. Li, Pinning synchronization of complex delayed dynamical networks via generalized intermittent adaptive control strategy, *Int. J. Robust Nonlinear Control*, **30**(1):421–442, 2020, https://doi.org/10.1002/rnc.4776.

14. S. Liu, L. Zhao, W. Zhang, X. Yang, F. E. Alsaadi, Fast fixed-time synchronization of T–S fuzzy complex networks, *Nonlinear Anal. Model. Control*, **26**(4):597–609, 2021, https://doi.org/10.15388/namc.2021.26.23060.

15. B. Lu, H. Jiang, C. Hu, A. Abdurahman, M. Liu, H_∞ output synchronization of directed coupled reaction-diffusion neural networks via event-triggered quantized control, *J. Franklin Inst.*, **358**(8):4458–4482, 2021, https://doi.org/10.1016/j.jfranklin.2021.03.007.

16. B. Mao, X. Wu, H. Liu, Y. Xu, J. Lü, Adaptive fuzzy tracking control with global prescribed-time prescribed performance for uncertain strict-feedback nonlinear systems, *IEEE Trans. Cybern.*, **54**(9):5217–5230, 2024, https://doi.org/10.1109/TCYB.2024.3366177.

17. M. Nikpour, P. B. Yousefi, H. Jafarzadeh, K. Danesh, R. Shomali, S. Asadi, A. G. Lonbar, M. Ahmadi, Intelligent energy management with IoT framework in smart cities using intelligent analysis: An application of machine learning methods for complex networks and systems, *J. Netw. Comput. Appl.*, **235**:104089, 2025, https://doi.org/10.1016/j.jnca.2024.104089.

18. G. Paukštaitė, A. Štikonas, Green's matrices for first order differential systems with nonlocal conditions, *Math. Model. Anal.*, **22**(2):213–227, 2017, https://doi.org/10.3846/13926292.2017.1291456.

19. D. Peng, X. Li, Leader-following synchronization of complex dynamic networks via event-triggered impulsive control, *Neurocomputing*, **412**:1–10, 2020, https://doi.org/10.1016/j.neucom.2020.05.071.

20. S. Roman, A. Štikonas, Third-order linear differential equation with three additional conditions and formula for Green's function, *Lith. Math. J.*, **50**(4):426–446, 2010, https://doi.org/10.1007/s10986-010-9097-x.

21. M. Shen, C. Wang, W. Qin, Q.-G. Wang, T. Huang, Fault-tolerant synchronization control for complex networks by an average observer approach, *IEEE Trans. Syst. Man Cybern. Syst.*, **55**(11):7705–7713, 2025, https://doi.org/10.1109/TSMC.2025.3598020.

22. H. Su, W. Zhang, Q. Zhang, Event-triggered adaptive tracking control for uncertain nonlinear systems with preassigned prescribed performance constraints under three cases, *Nonlinear Dyn.*, **113**:1245–1261, 2025, https://doi.org/10.1007/s11071-024-10269-8.

23. H. Tan, J. Wu, H. Bao, Event-triggered impulsive synchronization of fractional-order coupled neural networks, *Appl. Math. Comput.*, **429**:127244, 2022, https://doi.org/10.1016/j.amc.2022.127244.

24. Y. Tang, Y. Lv, J. Zhao, L. Jian, L. Li, Prescribed performance event-triggered optimal control of nonlinear multi-input systems, *Neurocomputing*, **637**:130044, 2025, https://doi.org/10.1016/j.neucom.2025.130044.

25. Y. Tian, G. Li, P. Sun, Information evolution in complex networks, *Chaos*, **32**(7):073105, 2022, https://doi.org/10.1063/5.0096009.

26. Z. Wang, L. Zhu, Pattern dynamics analysis and control strategies of rumor propagation model in complex networks based on real data, *Inf. Sci.*, **720**:122529, 2025, https://doi.org/10.1016/j.ins.2025.122529.

27. X. Wu, J. Wang, P. Li, X. Luo, Y. Yang, Internet of things as complex networks, *IEEE Netw.*, **35**(3):238–245, 2021, https://doi.org/10.1109/MNET.011.2000537.

28. Y. Xie, X. Li, X. Wang, Z. Ye, X. Hu, Y. Hu, Y. Jia, Synchronization of complex networks with synapse regulated by energy difference, *Nonlinear Dyn.*, **113**(10):12099–12115, 2025, https://doi.org/10.1007/s11071-024-10814-5.

29. J. Xu, Y. Liu, J. Qiu, J. Lu, Event-triggered impulsive control for nonlinear stochastic delayed systems and complex networks, *Commun. Nonlinear Sci. Numer. Simul.*, **140**:108305, 2025, https://doi.org/10.1016/j.cnsns.2024.108305.

30. X. Yang, A. Li, Q. Zhu, Dynamic periodic event-triggered control of stochastic complex networks with time-varying delays, *Neural Netw.*, **190**:107659, 2025, https://doi.org/10.1016/j.neunet.2025.107659.

31. Z. Yang, H. Shi, Q. Xiao, J. Zhang, J.-A. Wang, Fixed/preassigned-time synchronization of complex networks under event-dependent intermittent control, *Neurocomputing*, **666**:132315, 2026, https://doi.org/10.1016/j.neucom.2025.132315.

32. D. Yao, X. Xie, Prescribed performance practical fixed-time consensus control for multiagent systems with input saturation, *IEEE Trans. Syst. Man Cybern. Syst.*, **55**(7):4864–4876, 2025, https://doi.org/10.1109/TSMC.2025.3560029.

33. C. Zhang, X. Sun, H.-N. Wu, Z.-P. Wang, Resilient-triggered fault-tolerant fuzzy consensus for DPS-based MASs against multiple attacks and data compression, *Fuzzy Sets Syst.*, **524**:109643, 2026, https://doi.org/10.1016/j.fss.2025.109643.

34. C. Zhang, X.-Y. Sun, H.-N. Wu, Z.-P. Wang, Hybrid event-triggered fuzzy secure consensus for PDE-based multi-agent systems subject to time delays and multiple attacks, *IEEE Trans. Autom. Sci. Eng.*, **23**:5374–5386, 2026, https://doi.org/10.1109/TASE.2026.3665192.

35. N. Zheng, N. Han, N. Gunasekaran, Exponential stabilization of stochastic complex networks with Markovian switching topologies via intermittent discrete-time state observation control, *Nonlinear Anal. Hybrid Syst.*, **49**:101365, 2023, https://doi.org/10.1016/j.nahs.2023.101365.

36. H. Zhou, Y. Chen, D. Chu, W. Li, Impulsive stabilization of complex-valued stochastic complex networks via periodic self-triggered intermittent control, *Nonlinear Anal. Hybrid Syst.*, **48**:101304, 2023, https://doi.org/10.1016/j.nahs.2022.101304.

37. C. Zhu, B. Chang, Edge-based event-triggered output feedback control for stochastic multi-agent systems, *Int. J. Adapt. Control Signal Process.*, **38**(10):3346–3360, 2024, https://doi.org/10.1002/acs.3878.